Research in Pharmaceutical Sciences, October 2025; 20(5): 760-776
Received: 27-02-2025
Peer Reviewed: 01-04-2025
Revised: 03-06-2025
Accepted: 08-06-2025
Published: 20-10-2025

School of Pharmacy & Pharmaceutical Sciences
Isfahan University of Medical Sciences

Original Article

Hippocampal synaptic markers and cognitive recovery in spinal cord injury: the therapeutic potential of neural stem cell-laden carbon nanotube-based fiber scaffolds with liposomal hesperidin

Amirhossein Rabiei Rad[1], Tahere Mokhtari[2], Esmael Amirazodi[3], Amir Mahdi Molavi[4], Fatemeh Mortazavi Moghadam[5], Reza Kazemi Oskuee[6], and Arman Abroumand Gholami[7,8,9,*]

[1]*Faculty of Health Sciences, Department of Physiotherapy and Rehabilitation, Tokat Gaziosmanpaşa University, Tokat, Turkey.*
[2]*Department of Pathology, Division of Experimental Pathology, School of Medicine, University of Pittsburgh, Pittsburgh, Pennsylvania, USA.*
[3]*Department of Neurology, Ahvaz Jundishapur University of Medical Sciences, Ahvaz, Iran.*
[4]*Department of Materials Research, Iranian Academic Center for Education, Culture and Research, Khorasan Razavi Branch, Mashhad, Iran*
[5]*Department of Life Science Engineering, Faculty of New Sciences and Technologies, University of Tehran, Iran.*
[6]*Department of Medical Biotechnology and Nanotechnology, Faculty of Medicine, Mashhad University of Medical Sciences, Mashhad, Iran.*
[7]*Nervous System Stem Cell Research Center, Semnan University of Medical Sciences, Semnan, Iran.*
[8]*Tissue Engineering Research Group (TERG), Department of Anatomy and Cell Biology, School of Medicine, Mashhad University of Medical Sciences, Mashhad, Iran.*
[9]*Department of Neuroscience, Faculty of Medicine, Mashhad University of Medical Sciences, Mashhad, Iran.*

Abstract

Background and purpose: Spinal cord injury (SCI) causes motor and cognitive impairments, with secondary hippocampal damage contributing to memory deficits. This study examined the effects of neural stem cell (NSC)-laden polyurethane/functionalized multiwalled carbon nanotube (PU/f-MWCNT) scaffolds coated with liposomal hesperidin (Hsd@lip) on hippocampal synaptic integrity, neuroinflammation, and memory in a rat model of dorsal hemisection SCI.
Experimental approach: Electrospun PU/f-MWCNT scaffolds were prepared and loaded with NSCs, Hsd@lip, or both. Wistar rats (n = 15/group) were assigned to untreated SCI, scaffold+Hsd@lip (PCH), scaffold+NSC (PCN), or scaffold+NSC+Hsd@lip (PCHN). Four weeks post-implantation, hippocampal synaptic plasticity, oxidative stress, neuronal survival, and memory performance were evaluated using electrophysiology, biochemical assays, histology, and behavioral tests.
Findings/Results: The scaffolds were uniform, bead-free fibers with an average diameter of 174.7 ± 63.5 nm. Hsd@lip coating formed a thin, non-aggregated layer that maintained scaffold porosity. Cell seeding demonstrated good NSC adhesion and spreading, supporting the scaffold's biocompatibility. Compared to the SCI group, animals treated with PCHN exhibited a significant reduction in MDA levels and decreased AChE activity, and increased thiol content. Doublecortin expression markedly increased, while NF-κB levels and dark neuron counts significantly reduced. Furthermore, cognitive function improved.
Conclusion and implications: These findings highlight the potential of NSC-laden PU/f-MWCNT scaffolds coated with Hsd@lip to mitigate hippocampal damage, restore synaptic integrity, and improve cognitive function following SCI. This multimodal approach offers a promising therapeutic strategy for addressing the cognitive sequelae of SCI.

Keywords: Action potentials; Drug delivery systems; Memory; Neurogenesis; Stem cell therapy; Tissue engineering.

INTRODUCTION

One area of study within spinal cord injury (SCI) research focuses on the development of neurological and psychological disorders, cognitive deficits, and memory impairments (1-4).

*Corresponding author: A. Abroumand Gholami
Tel & Fax: +98-5138002470
Email: Aroma3162@gmail.com, Abroumanda981@mums.ac.ir

Access this article online	
	Website: http://rps.mui.ac.ir
	DOI: 10.4103/RPS.RPS_39_25

Similarly, individuals with SCI are 13 times more likely to experience cognitive disorders, particularly difficulties in learning new tasks and forming new memories, accompanied by reduced processing speed, verbal fluency, visual memory, and perceptual reasoning (5). Therefore, one hypothesis suggests that cognitive deficits and memory reduction in individuals with SCI, compared to age-matched healthy individuals, may be due to decreased hippocampal neurogenesis (2,6). Furthermore, the brains of injured animals are not immune to these inflammatory changes, indicating that SCI affects cell cycle function and leads to widespread neurotoxicity in various brain regions (4,7,8). On the other hand, these inflammatory changes are associated with deficits in spatial memory (1,9). Following SCI, in addition to cell loss in various hippocampal regions, the number of Doublecortin-positive (DCX^+) cells in the hippocampus decreases, confirming the impairment of hippocampal neurogenesis caused by SCI (10,11).

Biomaterial scaffolds can create a structural platform and bridge the SCI gap to facilitate axonal growth across the injury site (12,13). In addition to providing physical support and spatial guidance, biomaterials can also be utilized to deliver stem cells and bioactive molecules to create a favorable microenvironment at the SCI site (14-16). Various types of scaffolds, differing in spatial structure, mechanical strength, and biodegradability, have been developed for SCI repair in animal models, showing promising therapeutic effects (17-19). However, there are no commercially available biomaterial products that have been globally approved for treating SCI patients.

Nanofibrous scaffolds play a crucial role in supporting neuronal functions by providing contact guidance for cell growth, neurite outgrowth, and capillary formation, which aids in cell orientation, proliferation, differentiation, and migration (18). Among the materials used, polyurethane (PU) stands out for its excellent biocompatibility, appropriate biodegradability, and non-toxic properties, along with high compressive strength and toughness, making it suitable for neural applications (12,15,20,21). However, some PU-based scaffolds, such as the porous nerve conduit developed by Cui *et al.*, have shown limitations in elastic properties (22). To address these challenges, carbon-based materials, particularly carbon nanotubes (CNTs), have been incorporated into scaffolds. CNTs enhance porosity, surface-to-volume ratio, electrical conductivity, and mechanical strength, while also improving hydrophilicity, cell infiltration, and cellular compatibility (16,20,23). These properties make CNT-based nanofibrous scaffolds highly effective in supporting neuronal growth, differentiation, and synapse formation, positioning them as promising candidates for neural tissue engineering and the design of neural prosthetics (19,20). Despite these advancements, engineered scaffolds by themselves cannot fully address the extensive secondary damage caused by SCIs; they are primarily beneficial as a support for drug or cell therapies.

Recently, neural stem cells (NSCs) have been widely utilized in SCI research as seed cells due to their potential for replacing damaged spinal tissue through proliferation and differentiation, and/or providing nutritional support for repair (13,24). Some studies indicate that newly differentiated neurons can participate in neurotransmission and facilitate the activity of surviving host axons above and below the injured segments, thereby improving motor function (12,18). However, SCI leads to the secretion of several pro-inflammatory factors, such as lipid peroxidation and tumour necrosis factor alpha (TNF-α) at the injury site, which can extend to brain regions (8,12,25,26). This process induces inflammatory responses that slow down the repair process in the injury area, potentially resulting in the loss of transplanted cells at the site of injury (13,14,23). Therefore, it is believed that reducing inflammation could promote the regeneration of damaged tissue and preserve transplanted cells within the host (27,28).

Hesperidin (Hsd) is a natural bioflavonoid glycoside with antioxidant, anti-inflammatory, and neuroprotective properties, making it a promising candidate for neural regeneration therapies (29,30). It promotes neuronal survival and differentiation by activating key signaling pathways such as MAPK and PI3K (31,32), while also reducing oxidative stress and

inflammatory responses by scavenging free radicals and lowering pro-inflammatory cytokines like interleukin-1β and TNF-α (33). These properties are particularly beneficial in the context of SCI, where Hsd has been shown to reduce neuronal and axonal death while supporting regeneration (16,27). Importantly, studies have shown that Hsd can mitigate apoptosis in hippocampal regions such as CA1 and CA3, enhance neurogenesis in the dentate gyrus (DG), and improve spatial memory and learning abilities (29-31,34).

However, the direct application of Hsd in tissue engineering is limited by its poor solubility, low bioavailability, and instability under physiological conditions (35). To overcome these challenges, liposomal encapsulation (Hsd@lip) has emerged as an effective strategy (36). Liposomes enhance the solubility, stability, and controlled release of Hsd, ensuring prolonged therapeutic effects (37,38). Additionally, they improve cell-scaffold interactions by increasing scaffold hydrophilicity and promoting cell adhesion, which are critical for neural tissue engineering (39). By integrating Hsd@lip into biomaterial scaffolds, a favorable microenvironment can be created to enhance cell survival, neurite outgrowth, and synaptic plasticity, ultimately supporting functional recovery in SCI and mitigating secondary hippocampal damage and cognitive impairments (40).

This study aimed to investigate the therapeutic potential of a combined approach using CNT-based nanofibrous scaffolds, Hsd@lip, and NSCs for the treatment of hippocampal damage following SCI. By simultaneously addressing spinal cord repair and preventing cognitive and memory impairments associated with SCI, this study provides a comprehensive strategy for improving both motor and cognitive functions following SCI.

MATERIALS AND METHODS

Preparation of Hsd@lip

Drug-loaded liposomes were synthesized using the remote loading method (40). Briefly, lipids are composed of hydrogenated soy phosphatidylcholine (HSPC), cholesterol (Chol), and distearoyl-glycero-3-phosphoethanolaminemethoxy polyethylene glycol2000 (DSPEmPEG2000; Avanti Polar Lipids, Alabaster, USA) in a molar ratio of 50:40:10, dissolved in chloroform (20 mL; Merck, Germany) and evaporated under reduced pressure to form a thin lipid film. The liposomes were then extruded through polycarbonate membrane filters (Sigma Aldrich, St. Louis, Missouri, USA) with pore sizes of 200 nm and 100 nm to reduce their size. After dialysis, a solution of Hsd (Sami Labs Limited, Bengaluru, Karnataka, India) in dextrose (10 mg/mL) was added, and the mixture was incubated at 60 °C for 2 h. Unencapsulated Hsd was removed by centrifugation (7500 rpm, 10 minutes), and the resulting Hsd@lip was collected and stored at 4 °C until further use. The mean particle size, polydispersity index (PDI), and zeta potential of Hsd@lip were determined using dynamic light scattering (DLS) with a Zetasizer Nano ZS (Malvern Instruments, UK) at 25 °C. Encapsulation efficiency was assessed by centrifugation at 7500 rpm for 10 min to separate free Hsd, followed by spectrophotometric analysis of the supernatant at 285 nm.

Electrospinning of scaffolds

A PU/multi-walled CNT solution was created by ultrasonically mixing multi-walled carbon nanotubes (MWNTs; US Research Nanomaterials, Inc., USA) in tetrahydrofuran for 30 min and vortexing for 2 h. This solution was combined with a PU (Sigma-Aldrich, USA) solution in dimethylformamide, stirred for 24 h, with a final solvent ratio of 1:1 (v/v) and a PU concentration of 20% (w/v); MWNTs were at 2% (g/g) of PU. For electrospinning, the solution was loaded into a 23-gauge syringe. The process used an electrospinning machine (Fanavaran Nano-Meghyas Co., Iran), with parameters set to a 15 cm needle-to-collector distance, 18 kV voltage, 1 mL/h flow rate, and 800 rpm collector rotation. Conducted at room temperature and about 25% humidity, the aluminum foil collector was removed after 24 h, and the dried mat was carefully peeled off.

Cell seeding

The NSC lines derived from embryonic neural tissue (Histogenotech, Iran) were grown in Dulbecco's modified Eagle's medium (DMEM; Gibco, Massachusetts, USA) enriched with 10% fetal bovine serum (FBS, Gibco, Thermos Fisher Scientific, US) at 37 °C in a humidified environment containing 5% CO_2. Once they reached 80% confluence, the NSCs were subcultured using 0.25% trypsin (Gibco, Thermo Fisher Scientific, US), and cells from the fourth passage were utilized for subsequent experiments.

SCI induction

In this study, sixty female Wistar rats weighing 250-300 g were utilized. The rats were housed individually in cages with a 12/12-h light-dark cycle, and they had unrestricted access to food and water. Animal welfare was monitored, and all surgical procedures adhered to the ethical guidelines set by Mashhad University of Medical Sciences (MUMS) under COD number (IR. MUMS. REC.1399.571). Anesthesia was achieved through intraperitoneal (IP) injection of a mixture of xylazine (5 mg/kg) and ketamine (100 mg/kg). The dorsal skin was shaved and disinfected with betadine solution. A midline incision was made, followed by a T9 laminectomy using a rongeur. The dura mater was exposed, incised lengthwise, and retracted. A 1-mm segment of dorsal hemisection spinal tissue between the T8 and T9 vertebrae was excised with microdissection scissors and a 22-gauge needle. Before implantation, the PU/f-MWCNT scaffold was sterilized under UV light for 1 h. Scaffolds, with or without NSCs and Hsd@lip, were implanted into the spinal cord and muscle, and the incisions were closed with absorbable Vicryl sutures. The scaffolds measured 6 × 3 mm, and the volume of Hsd@lip used was 50 µL.

The animals were randomly divided into four groups (n = 15/group), including (1) SCI without treatment (Ctrl); (2) laminectomy rats receiving scaffolds with Hsd@lip (PCH), where Hsd at 32.5 µg/mL was applied to the scaffold surface for two days, and liposomes of the same concentration and volume were added 30 min before implantation; (3) SCI with scaffolds containing NSCs (PCN), where 10^4 NSCs were seeded on the scaffold for two days before grafting; (4) SCI with liposomes + scaffolds containing NSCs (PCHN), where Hsd@lip was applied to the scaffold, NSCs were seeded for two days, and Hsd@lip was added 30 min before grafting.

The four-week time point was selected based on previous studies indicating that this duration represents a sub-chronic phase of SCI, during which secondary injury mechanisms such as inflammation, glial scar formation, axonal degeneration, and early stages of tissue remodeling are well established (42). This window allows for meaningful evaluation of both pathological progression and the therapeutic effects of biomaterials or drugs. Furthermore, by four weeks post-injury, spontaneous recovery typically plateaus, enabling more accurate assessment of treatment efficacy on structural and functional outcomes.

Behavioral assessments

In this study, a shuttle box apparatus was utilized to assess learning and memory through the PA test. The shuttle box consists of two chambers, one illuminated and one dark, each measuring 20 × 20 × 30 cm, separated by a guillotine door. The floor of the dark chamber is equipped with steel rods spaced 1 cm apart. An electric shock, set at an intensity of 2 mA and lasting 2 s at a frequency of 50 Hz, is administered to these rods *via* a stimulator. The experiment comprises three phases. The first phase is the familiarization period, during which the animal is placed in the illuminated chamber for two days. After 15 s, the guillotine door opens, and the latency to enter the dark chamber, as well as the total time spent in both the dark and illuminated chambers over a duration of 300 s, is recorded. The second phase is the training period. In this phase, each mouse is placed in the illuminated chamber, and upon entering the dark chamber, the guillotine door closes. An electric shock of 2 mA for 2 s at a frequency of 50 Hz is then applied to the mouse's feet resting on the rods. This shock is administered solely during the training phase, after which all animals are returned to their cages. The third phase is the

testing period, conducted at 3-, 24-, 48-, and 72-h post-shock. The animal is again placed in the illuminated chamber, and the latency to enter the dark chamber, along with the total time spent in both light and darkness over a 300 s period, is recorded.

Electrophysiological recording methodology

In accordance with the protocols established by Abroumand Gholami *et al*., we prepared the subjects for electrophysiological assessments four weeks after SCI induction (40). Anesthesia was administered *via* urethane at a dosage of 1.6 g/kg, and the rats' heads were secured in stereotaxic apparatuses to ensure stability during the procedure. We accurately identified the locations of the CA1 region and the pathways of the pyramidal cells on the skull (43). A bipolar stimulating electrode, constructed from stainless steel with a diameter of 100 µm and a tip separation of 500 µm (CFW, USA), was carefully positioned within the pyramidal cell layer. Concurrently, a recording electrode made of tungsten, measuring 50 µm in diameter with a tip separation of 1 mm (CFW, USA), was inserted into the CA1 region, guided by the following coordinates: anterior-posterior (AP) = 3.4 mm, medial-lateral (ML) = 1.5 mm, and dorsal-ventral (DV) = 4.45 mm, at an angle of 52.5°. To capture the synaptic input associated with field excitatory postsynaptic potentials (fEPSPs), we employed a 2-channel electromodule amplifier (R12, ScienceBeam, Tehran, Iran). Following a stable baseline recording of synaptic responses maintained for 30 min, long-term potentiation (LTP) was induced through tetanic stimulation, consisting of 100 pulses delivered at a frequency of 100 Hz. Synaptic responses were subsequently recorded 90 min after the LTP induction, with changes in response quantified as a percentage of the baseline amplitude.

Biochemical investigations

In the fourth week of the study, following the completion of electrophysiological assessments, the animals were anesthetized for deep sedation using ketamine (90 mg/kg) and xylazine (10 mg/kg). To evaluate oxidative stress markers, a total of seven rats from each group were randomly selected. Their brains were extracted through sagittal and coronal incisions, and the hippocampus was isolated. The collected samples were stored at -20 °C. For biochemical analyses, the samples were homogenized in a 10% potassium chloride solution to assess acetylcholinesterase (AchE) and oxidative stress factors, including total thiols (-SH), malondialdehyde (MDA), and superoxide dismutase (SOD). Finally, the homogenized samples were centrifuged, and the supernatant was collected for the measurement of biochemical indices. Further details regarding each test can be found in the supplementary file (Biochemical evolution section).

Histochemical and immunohistochemical assessment

Eight rats from each group were randomly selected for histological analysis. Following anesthesia, their brains were extracted and fixed in 10% neutral formalin (Merck, Germany). After 72 h in the fixative, the samples underwent dehydration through ascending grades of alcohol (80%, 90%, 95%, and 100%; Merck, Germany), with each grade maintained for 2 h. Clearing was performed using xylene (Merck, Germany), followed by infiltration in molten paraffin at 58-60 °C for 1.5 h across three paraffin containers. The samples were then placed in rectangular molds and sectioned using a rotary microtome, producing coronal sections of 5-µm thickness with 15-µm spacing, resulting in 30 slides/block. Toluidine blue (TB) staining (Sigma-Aldrich, St. Louis, MO, USA) was employed to identify dark neurons, while immunohistochemical staining was utilized to assess markers of neurogenesis and inflammation. One section from each of three consecutive sections was analyzed for each staining procedure.

For TB staining, the samples were deparaffinized in xylene, rehydrated through descending grades of alcohol, and stained with TB for 1 to 3 min. After washing and rehydration, the samples were mounted with Entellan. During microscopic examination, nuclei that stained dark blue were classified as dark neurons.

In this study, immunohistochemical staining was utilized to identify the neurogenesis marker DCX and the inflammatory marker nuclear factor kappa-light-chain-enhancer of activated B cells (NF-kB) in the subgranular zone (SGZ) of the dentate gyrus. The procedure involved deparaffinization with xylene, rehydration through descending alcohol grades, and antigen retrieval using heat. Following blocking with 1% bovine serum albumin (Sigma-Aldrich, St. Louis, MO, USA), samples underwent incubation with primary (anti-DCX and anti-NF-kB; Abcam, Cambridge, UK) and secondary antibodies (horseradish peroxidase (HRP)-conjugated; Abcam, Cambridge, UK). The samples were then treated with 3, 3′ diaminobenzidine (DAB) solution for visualization. Cells exhibiting dark brown-stained nuclei were classified as NF-kB positive, while those with dark brown-stained cytoplasm were identified as DCX positive. Details of the cell counting method are listed in the supplementary file (Cell counting method section).

Statistical analysis

All graphs and statistical analyses were performed using GraphPad Prism version 9.0 (GraphPad Software, San Diego, CA, USA). Data were analyzed using one-way or two-way ANOVA, depending on the experimental design. One-way ANOVA followed by Tukey's post hoc test was applied for comparisons among treatment groups in biochemical and histological assays. Two-way ANOVA was used for behavioral and electrophysiological assessments. Correlations between variables were evaluated using simple linear regression. Data are expressed as mean ± SEM.

RESULTS

Visualization of Hsd@lip and NSCs on PU composite fibers

The synthesized Hsd@lip exhibited a mean size of 105.84 ± 37.71 nm with a PDI of 0.21 ± 0.11, indicating uniformity. The encapsulation efficiency reached 76%, and the zeta potential was −20.3 ± 6.7 mV. Figure 1 illustrates the morphology of the electrospun fibers in three distinct conditions: without Hsd@lip loading, with Hsd@lip loading, and following cell seeding after Hsd@lip incorporation. The analysis revealed an average fiber diameter of 174.7 ± 63.5 nm. The morphology of the scaffold exhibited fibers that were free from beads and aggregation (Fig. 1A). Additionally, the Hsd@lip loading process did not result in liposome aggregation. The liposomes formed a thin layer covering the extensive surface area of the scaffold, contributing to the extracellular matrix (ECM)-like structure while preserving the scaffold's porosity (Fig. 1B). Figure 1C demonstrates the spreading of cells across the fibers, with the flattened morphology of the cells suggesting that the scaffold surface is conducive to the growth and adhesion of NSCs.

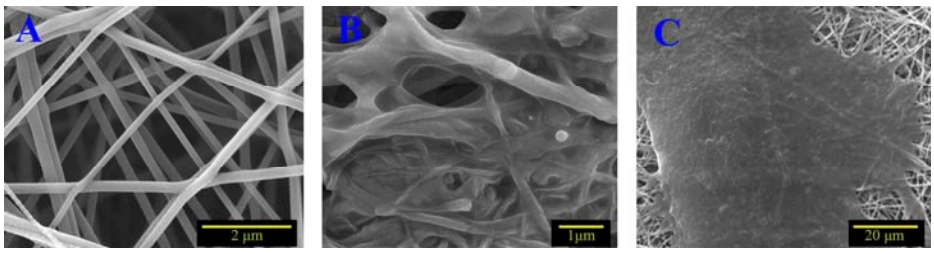

Fig. 1. Microscopic images of (A) PU/f-MWCNT fibers, (B) Hsd@lip-enrich scaffold, and (C) seeding of neural stem cells on the PU/f-MWCNT/Hsd@lip scaffolds. PU, Polyurethane; f-MWCNT, functionalized multiwalled carbon nanotube; Hsd@lip, liposomal hesperidin.

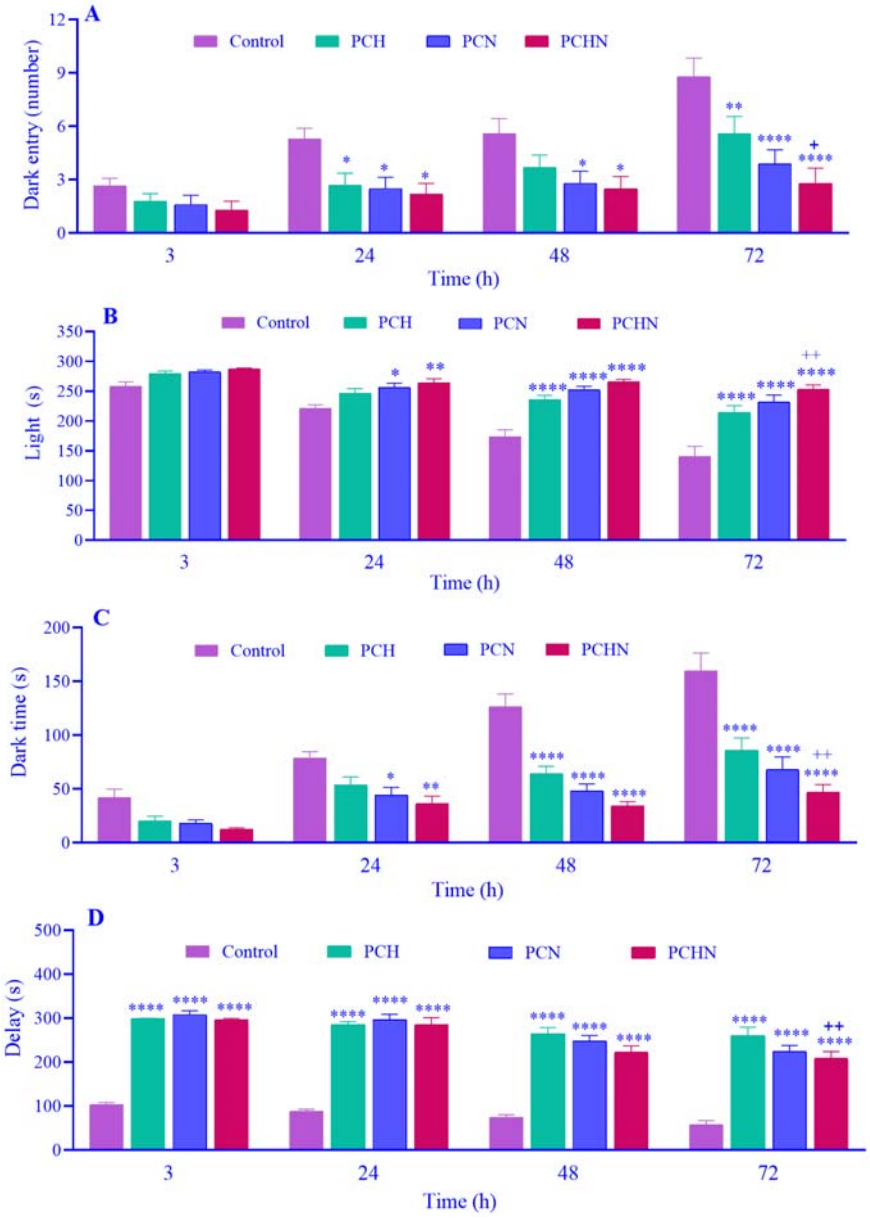

Fig. 2. Memory behavior was evaluated by measuring inescapable memory four weeks after dorsal hemisection in the control, PCH, PCN, and PCHN groups. The assessed parameters included (A) the number of entries by the animals into the dark chamber, the time spent in the (B) light or (C) dark chamber, and (D) the entry latency. The data are presented as mean ± SEM, n = 10. *P < 0.05, **P < 0.01, and ****P < 0.0001 indicate significant differences compared to the control group at each time point; ^{+}P < 0.05 and ^{++}P < 0.01 versus the PCH group. SCI, Spinal cord injury; PU, polyurethane; f-MWCNT, functionalized multiwalled carbon nanotube; Hsd@lip, liposomal hesperidin; PCH, SCI animals receiving PU/f-MWCNT/Hsd@lip scaffolds; PCN, SCI animals receiving PU/f-MWCNT/NSCs scaffolds, and PCHN, SCI animals receiving PU/f-MWCNT/Hsd@lip/NSCs scaffolds.

Impact of combination scaffold implantation at the SCI site on avoidance memory

In the fourth week of the study, following the attainment of a stable condition in the rats, a memory assessment was conducted using the passive avoidance test (the evaluation of hind limb motor function is provided in the supplementary file- Fig 1S). The indices evaluated included the number of entries into the dark chamber, the time spent in the light/dark chamber, and the delay in

entry time (Fig. 2A-D). Observations of the changes in these indices within the control group indicate memory impairment after SCI. The results demonstrate that the therapeutic intervention across all groups reduced the number of entries into the dark chamber compared to the control group. Notably, a significant decrease in this parameter was observed in the PCHN group relative to the PCH group after 72 h. However, no other significant differences were detected among the intervention groups. The time spent in the light chamber during the first 24 h of the experiment exhibited a significant increase solely in the PCHN and PCN groups compared to the control group. Additionally, on the second and third days, the PCH group showed a substantial increase in this parameter compared to the control group. A statistically significant difference was noted between the PCHN and PCH groups on the third day. The results indicated that the time spent in the dark chamber was significantly reduced compared to the control group, maintaining a consistent significance level as observed in the previous parameter for all treatment groups. The duration of the entry delay was the only parameter that exhibited a clear distinction in the scaffold-receiving groups compared to the control group during the initial three hours. This parameter indicated that the scaffold implant was associated with increased delay in entry across all four time points examined. Furthermore, at the fourth time point of the experiment, a significant difference was observed in the delay in entry for the PCHN group compared to the PCH group.

Enhancement of hippocampal LTP post-combination scaffold implantation in SCI

Figure 3 illustrates the changes in LTP observed four weeks after the induction of the model in the study groups. Following high-frequency stimulation, an increase in the percentage of changes in the baseline fEPSP amplitude was recorded across all groups (Fig. 3A). At baseline (before HFS), the fEPSP amplitudes of all experimental groups (PCH, PCN, and PCHN) did not differ significantly from the control SCI group.. However, at all recorded time points following high-frequency stimulation, a significant decrease in the percentage of fEPSP amplitude changes was noted in both the PCN and PCHN groups relative to the control group. Additionally, a significant reduction in these changes was observed in the PCHN group compared to the PCH group. Furthermore, the data presented in Fig. 3B depict the total percentage of changes in the recorded amplitude compared to baseline after high-frequency stimulation, averaged over 90 min. These results demonstrate a significant decrease in these levels in the PCN and PCHN groups when compared to the control group. A similar decrease was also observed between the PCHN and PCH groups.

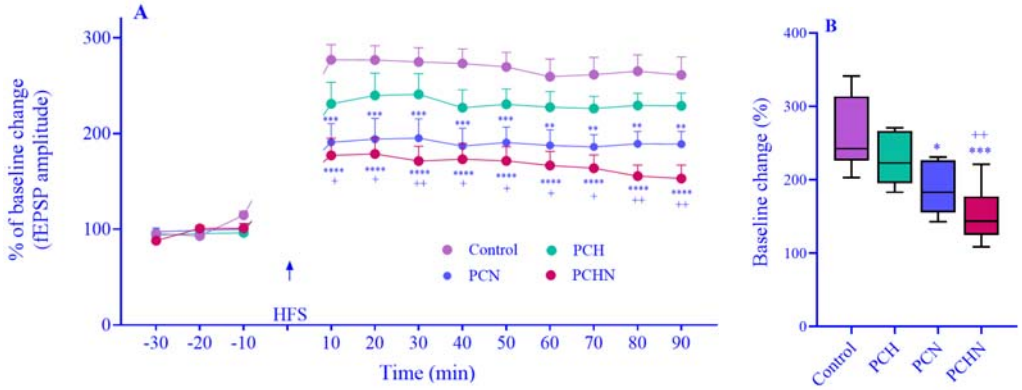

Fig. 3. (A) The dot-connecting line plot illustrates the percentage change in the amplitude of electrophysiological recordings following HFS compared to baseline measurements in the control, PCH, PCN, and PCHN groups within the Schaffer collateral pathway of the hippocampus after SCI at the end of the fourth week. (B) The box-and-whisker plot displays the percentage change from baseline in 90-min long-term potentiation recordings in the animals. The data are presented as mean ± SEM, n = 7. *$P < 0.05$, **$P < 0.01$, ***$P < 0.001$, and ****$P < 0.0001$ indicate significant differences compared to the control group; $^{+}P < 0.05$ and $^{++}P < 0.01$ indicate significant differences compared to the PCH group. HFS, high-frequency stimulation; SCI, spinal cord injury; PU, polyurethane; f-MWCNT, functionalized multiwalled carbon nanotube; Hsd@lip, liposomal hesperidin; PCH, SCI animals receiving PU/f-MWCNT/Hsd@lip scaffolds; PCN, SCI animals receiving PU/f-MWCNT/NSCs scaffolds; PCHN, SCI animals receiving PU/f-MWCNT/Hsd@lip/NSCs scaffolds.

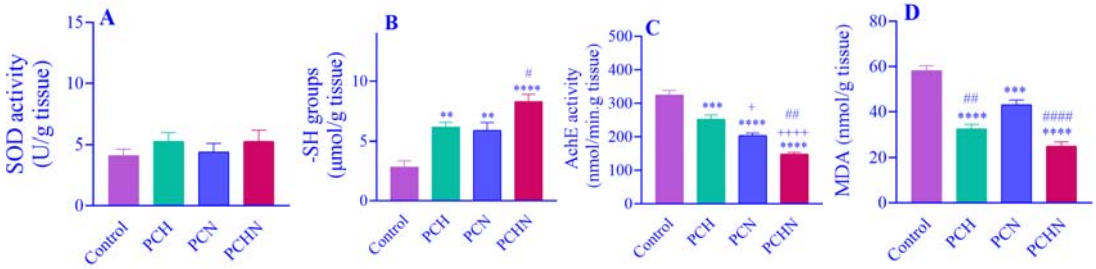

Fig. 4. The graphs display the levels of (A) SOD, (B) -SH, (C) AChE, and (D) MDA in the hippocampal tissue of the study groups four weeks post-spinal cord injury. The data are presented as mean ± SEM, n = 7. $^{*}P < 0.05$, $^{**}P < 0.01$, $^{***}P < 0.001$, and $^{****}P < 0.0001$ indicates significant differences compared the control group; $^{+}P < 0.05$ and $^{++}P < 0.01$ versus the PCH group; $^{\#}P < 0.05$, $^{\#\#}P < 0.01$, and $^{\#\#\#\#}P < 0.0001$ against PCN group. SCI, spinal cord injury; PU, polyurethane; f-MWCNT, functionalize-multiwalled carbon nanotube; Hsd@lip, liposomal hesperidin; PCH, SCI animals receiving PU/f-MWCNT/Hsd@lip scaffolds; PCN, SCI animals receiving PU/f-MWCNT/NSCs scaffolds, and PCHN, SCI animals receiving PU/f-MWCNT/Hsd@lip/NSCs scaffolds; SOD, superoxide dismutase; -SH, thiol groups; AChE, acetylcholinesterase; MDA, malondialdehyde.

Combination scaffold implantation modulates hippocampal oxidative status and neurotoxicity following SCI

Figure 4 presents the biochemical factors in hippocampal tissue following the induction of the SCI model after four weeks. Our results indicated no significant changes in SOD levels in hippocampal tissue post-SCI (Fig. 4A). The implantation of scaffolds in the spinal cord resulted in a significant increase in -SH levels in the PCH, PCN, and PCHN groups when compared to the control group (Fig. 4B). Additionally, a significant increase in -SH levels was observed in the PCHN group compared to the PCH group. Changes in AChE activity demonstrated that SCI led to an increase in the activity of this enzyme (Fig. 4C). The implantation of scaffolds in the spinal cord resulted in a decrease in AChE activity across all groups receiving scaffolds compared to the control group. A significant reduction in AChE activity was also noted in the hippocampal tissue of the PCN and PCHN groups compared to the PCH group. Furthermore, a significant difference in the decrease of AChE activity was observed between the PCHN and PCN groups. MDA levels in hippocampal tissue increased following SCI (Fig. 4D). Treatment with scaffolds in the PCH, PCN, and PCHN groups resulted in a significant decrease in MDA levels compared to the control group. Notably, a significant reduction in MDA levels was also observed in the PCH and PCHN groups compared to the PCN group.

Implantation of a combination scaffold enhances protein expression in hippocampal neurons following SCI

Figure 5A presents the histological and immunohistochemical results from the SGZ of the hippocampus, focusing on the assessment of dark neurons (TB staining), the inflammatory marker (NF-κB), and the neurogenesis marker (DCX) following SCI. The quantification of the neurogenesis marker revealed that scaffold implantation significantly enhanced the expression levels of DCX protein in the treated groups compared to the control group (Fig. 5B). Notably, a more pronounced increase was observed in the PCHN group relative to the PCH group. Quantification of TB staining indicated a decrease in the number of dark neurons in the PCH, PCN, and PCHN groups compared to the control group. Additionally, a significant reduction in dark neurons was noted in the hippocampal tissue of the PCHN group compared to both the PCH and PCN groups (Fig. 5C). The quantification of the inflammatory marker NF-κB in hippocampal tissue demonstrated a decrease in its expression in the PCH, PCN, and PCHN groups compared to the control group. Furthermore, a significant difference in the reduction of NF-κB expression was observed in the PCHN group compared to the PCN group (Fig. 5D).

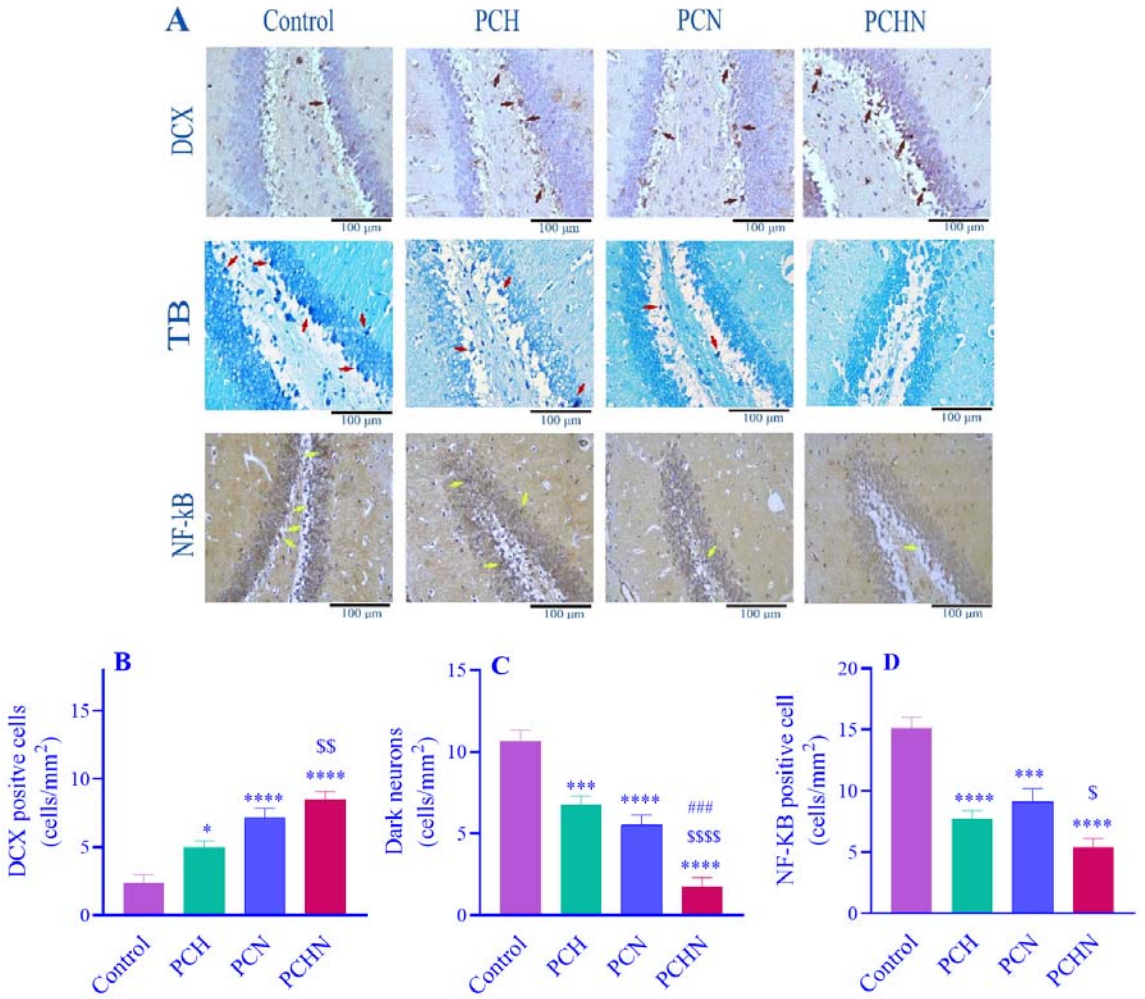

Fig. 5. (A) The micrographs display immunohistochemical sections for the DCX and NF-κB markers, along with TB staining in the subgranular zone of the hippocampus following SCI. The green, red, and yellow arrows indicate DCX-positive cells, dark neurons, and NF-κB-positive cells, respectively. Quantification of the number of (B) DCX-positive cells, (C) dark neurons, and (D) NF-κB-positive cells is presented. The data are presented as mean ± SEM, n = 8. *$P < 0.05$, ***$P < 0.001$, and ****$P < 0.0001$ indicates significant differences compared the control group; $^{\$}P < 0.05$, $^{\$\$}P < 0.01$, and $^{\$\$\$\$}P < 0.0001$ against PCH group, $^{\#\#\#\#}P < 0.001$ against PCN group. SCI, spinal cord injury; PU, polyurethane; f-MWCNT, functionalized multiwalled carbon nanotube; Hsd@lip, liposomal hesperidin; PCH, SCI animals receiving PU/f-MWCNT/Hsd@lip scaffolds; PCN, SCI animals receiving PU/f-MWCNT/NSCs scaffolds, and PCHN, SCI animals receiving PU/f-MWCNT/Hsd@lip/NSCs scaffolds; DCX, doublecortin; NF-κB, nuclear factor kappa-B; TB, toluidine blue.

DISCUSSION

Memory and hippocampal impairment following SCI is a crucial area of research for understanding the complex consequences of this condition. Research indicates that up to 64% of those affected by SCI experience some form of cognitive impairment, frequently worsened by comorbid conditions such as depression (11). The mechanisms behind these cognitive declines are multifaceted, involving inflammatory responses, apoptosis, and reduced neurogenesis in the hippocampus, all of which contribute to difficulties in memory retention and spatial navigation (2,26,44). Importantly, while SCI does not directly lead to memory loss, the interaction of various factors, including secondary complications and the specific brain regions impacted by the injury, creates an environment that can severely hinder cognitive health (7). Ongoing research aims to unravel these interrelationships, focusing on the

pathways that connect SCI to cognitive decline and exploring potential therapeutic interventions to mitigate these effects (8,25). As illustrated in Fig. 6, the implantation of a PU/f-MWCNT fibrous scaffold optimized with Hsd@lip and seeded with NSCs created a neuronal niche that effectively mitigated hippocampal damage after SCI. This multimodal platform reduced oxidative stress and acetylcholinesterase activity, suppressed neuroinflammation, decreased dark neurons, and enhanced neurogenesis (increased DCX expression). These changes were accompanied by improved long-term potentiation and memory performance, confirming both structural and functional recovery. Importantly, while several biochemical and behavioral parameters were improved, SOD levels in hippocampal tissue remained unchanged in our model, highlighting the specificity of the scaffold's effects.

Conductive scaffolds have been proposed as a niche to enhance stem cell behavior in the challenging conditions of the injured spinal cord (28). This concept has implications that extend beyond cell transplantation; these scaffolds have also been integrated into educational models designed to promote stem cell behavior (45). The potential of PU-based cell delivery systems, particularly when combined with CNTs, has been widely explored in the context of neural regeneration (12,23). Additionally, the physical characteristics resulting from the topology and surface structure of electrospun fibers significantly affect cellular signaling pathways, providing a solid foundation for their use in tissue grafting applications. Shrestha *et al.* noted that the physicochemical properties of PU/f-MWCNT fibers, such as electrical conductivity, mechanical strength, and optimal cell compatibility, make them ideal substrates for natural ECM, playing crucial roles in neural tissue engineering (20). In this study, we utilized PU/f-MWCNT composite fibers for neural tissue engineering to repair SCIs. We enhanced the surface with Hsd@lip to mimic the ECM and boost the antioxidant capacity and neuroprotection of the platform, facilitating the transfer of NSCs to the host tissue.

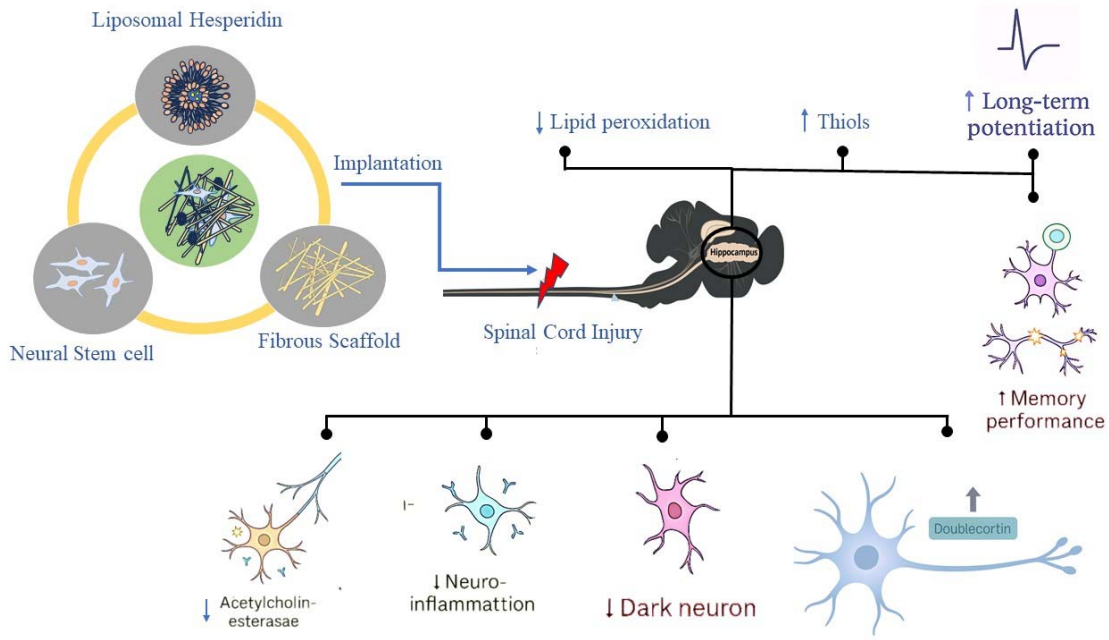

Fig. 6. Schematic representation of the neuroprotective effects of neural stem cell-laden PU/f-MWCNT scaffolds coated with liposomal hesperidin (Hsd@lip) in a rat model of spinal cord injury. The combinatorial approach reduced lipid peroxidation, acetylcholinesterase activity, neuroinflammation, and dark neurons, while enhancing thiol levels, Doublecortinexpression, long-term potentiation, and memory performance.

A key aspect of SCI is its effect on the electrophysiological properties of the hippocampus. Kalkhoran *et al.* suggested that the impairment of hippocampal LTP after SCI is caused by the blockade of NMDA receptors by secondary injury cascades (11). Our study confirmed the impairment of action potential recordings in hippocampal neurons post-SCI, noting changes in amplitude following HFS in treatment groups. The restoration of bioelectric signal transmission in the injured spinal cord has been linked to the synergistic effects of Hsd on cell-laden CNT composites (16). Although the implantation of PU fibers reinforced with CNTs improved spinal cord tissue structure, enhancing myelin regeneration and reducing inflammatory cells in the dorsal horn, this approach did not effectively compensate for changes in fEPSP amplitude recordings compared to cell implantation on scaffolds. However, our previous study indicated that CNT-based scaffolds did not significantly affect the slope and amplitude of hippocampal neuronal potential recordings, despite restoring gene expression related to synaptogenesis (40). We hypothesized that CNT-based fibers could optimize electrophysiological recordings due to their neuro-signaling and oxidative scavenging properties, enhanced by Hsd. This hypothesis is supported by studies highlighting Hsd's role in promoting synaptogenesis and enhancing action memory in the hippocampus (30-32).

In this study, we shifted our focus from merely assessing scaffold performance to using fibers for drug delivery and cell retention. Seeding NSCs on polymer scaffolds in the SCI improved connectivity in damaged neural circuits distant from the lesion (14). Our observations indicated that action potential impairments were compensated in groups receiving cell-laden scaffolds, with/without liposomes. The combined scaffold showed potential in improving synaptic potential impairments compared to groups receiving only liposome-enriched scaffolds. These findings are particularly significant given that SCI is believed to inactivate NSCs in hippocampal tissue (4). Evidence suggests that transplanting NSCs into injured CNS regions can promote the survival of hippocampal neurons and mitigate hippocampal-dependent spatial memory deficits, even when the injury site is distant from the hippocampus (45).

The pathophysiology following SCI involves primary and secondary injury processes, with oxidative stress playing a crucial role in exacerbating neuronal injury and hindering recovery. We measured lipid peroxidation, SOD, total thiol, and AChE levels in hippocampal tissue as markers of oxidative stress and neurotoxicity in chronic conditions post-acute SCI. We hypothesized that controlling these levels could mitigate secondary injury to the hippocampus caused by SCI. The idea that emerged from the increased neurotoxicity and oxidative status in the hippocampus following SCI (3,8). Platforms that incorporate CNTs implanted in the injured area of the spinal cord have been identified as an effective therapeutic approach. They work by modulating the formation of glial scars, which in turn helps regulate oxidative stress (16). Evidence shows that protecting intracellular thiol (sulfhydryl) content against oxidation, promoted by the Fe^{2+}-ascorbate system, increases linearly with the concentration of carbon-based nanomaterials, including CNTs (46). However, the low concentration of these materials in the electrospun fibers did not sufficiently control oxidative conditions related to SCI, prompting us to seek a multi-fold enhancement to address oxidative stress.

Our study demonstrated that scaffolds enriched with Hsd@lip improved oxidative stress markers in the hippocampus. Hsd appears to reduce oxidative stress and inflammation in SCI by regulating Nrf2/ARE/HO-1 and TGF-β/Smad3 signaling pathways (27). We also found that combined scaffolds with NSCs enhanced these improvements. The therapeutic effect of NSCs in acute SCI is often limited by the rapid loss of donor cells attributed to inflammation and oxidative stress. Yu *et al.* utilized a polylactic-co-glycolic acid scaffold, protected by a drug-releasing polymer, to enhance NSC viability in injured spinal cord tissue (47). Their findings indicated improved host microenvironment and NSC interaction, alongside modulation of inflammatory factors.

Thus, a reactive oxygen species-inhibiting substrate loaded with NSCs represents a promising strategy for treating SCI by addressing the adverse microenvironment.

Furthermore, we observed that increased levels of AChE in hippocampal tissue were associated with secondary injury. Our results revealed a strong correlation between impaired LTP and elevated AChE activity in the hippocampus (supplementary file, Fig. 4S). Evidence suggests that Hsd lowers AChE activity in the hippocampus under oxidative conditions, likely due to its anti-inflammatory properties (29). Furthermore, evidence indicates that NSC transplantation enhances cognitive performance in animal models by increasing hippocampal synaptic density and promoting the cholinergic system, mediated by reduced AChE activity (48). We observed similar improvements in LTP with reduced AChE activity in animals receiving the combined scaffold.

Based on these findings, the reduced activity of AChE resulting from the implantation of a scaffold filled with Hsd@lip alongside NSCs may enhance cholinergic neurotransmission efficiency due to an improved level of acetylcholine in the synaptic cleft, leading to enhanced LTP and, consequently improved cognitive function. Although we did not investigate the migration of stem cells to brain areas, it appears that the reduced AChE activity in animals receiving scaffolds containing stem cells plays a role beyond merely modulating inflammatory mediators and secretions. However, this hypothesis is beyond the scope of our study and remains unanswered. Notably, AChE responds to various insults, including oxidative stress. Based on these observations, we can suggest that the negative regulation of AChE following the administration of the combined scaffold may be mediated by the modulation of free radical production, lipid peroxidation, and, consequently, oxidative stress in the hippocampus.

A range of processes dependent on the hippocampus, including learning, memory, and mood regulation, relies on neurogenesis (49,50), which primarily occurs in the SGZ of the hippocampal DG in the adult brain (11). Growing evidence indicates that antioxidant and neuroprotective compounds can prevent hippocampal dysfunction by attenuating oxidative stress and improving memory performance in experimental models of neurodegeneration (51). Ying *et al*. found that SCI notably disrupts hippocampal neurogenesis, evidenced by a reduction in the number of immature DCX-positive neurons and mature NeuN-positive neurons (43). However, this negative impact can be counteracted with anti-inflammatory medications. Several studies have highlighted a protective role of Hsd in the hippocampus, showing that Hsd treatment increases the number of DCX-positive cells (52,53). Sato *et al.* also indicated that the anti-neuroinflammatory effects of Hsd are directly linked to the inhibition of NF-κB translocation and activity, as well as the downregulation of pro-inflammatory cytokines (53). Consistent with our findings, neuroprotective phytochemicals have also been shown to enhance hippocampal function and reduce oxidative stress. For example, treatment with crocin-loaded solid lipid nanoparticles significantly improved passive avoidance memory, reduced lipid peroxidation and pro-inflammatory cytokines, and increased antioxidant capacity and neurotrophic factors in epileptic rats (54). Our findings revealed that Hsd modulates inflammation and supports hippocampal recovery by reducing the number of dark neurons and NF-κB protein expression while increasing the number of DCX-positive neurons and repairing damaged spinal cord areas (data available in the supplementary file-Figs. 2S and 3S). Additionally, we discovered that the synergistic effects of neural stem cells in composite scaffolds enhance cognitive function by improving avoidance memory and neuromotor abilities.

However, careful planning is needed to examine the timing of responses (54). Since spinal injury models can only rarely allow such immediate interventions in clinical settings, and given that memory and cognitive dysfunction following spinal injury is not an immediate consequence that requires treatment right at the moment of injury, we suggested investigating therapeutic responses at various phases post-implantation and different stages after injury in future research. Our priority was to implant the

platform immediately after injury to avoid re-surgery, which could lead to significant survival gains in our animal model. The next step must be forward-looking; now that we understand the potential impact of composite scaffolds on different aspects of SCI, there is an urgent need to investigate the reproducibility of the treatment outcome with different injury induction models while carefully maintaining ethical considerations.

CONCLUSION

This study elucidates the intricate relationship between SCI and cognitive impairments, particularly emphasizing the role of neuroinflammation and hippocampal neurogenesis in memory function. Our findings demonstrate that the implantation of Hsd@lip-optimized CNT scaffolds significantly enhances memory retention and LTP in models of SCI. Moreover, the transplantation of NSCs onto these scaffolds showed promising results in promoting synaptic integrity and restoring cognitive functions, highlighting the potential of this combined therapeutic approach. The observed reduction in dark neurons within the hippocampus further supports the hypothesis that enhancing the neurogenic niche can counteract the detrimental effects of SCI on cognitive health. These scaffolds not only improved the biochemical environment of the injured tissue by mitigating oxidative stress and inflammation, as evidenced by reduced levels of MDA and enhanced -SH activity, but also positively modulated key neurobiological markers, including AChE, NF-kB, and DCX. In conclusion, the synergistic application of Hsd@lip scaffolds and NSCs represents a viable strategy for addressing cognitive deficits following SCI. Future studies should further explore the long-term histological and cognitive outcomes associated with this approach, including chronic neuroplasticity and behavioral improvements. Additionally, investigations into the optimization of scaffold architecture, controlled drug release kinetics, and targeted delivery mechanisms will be essential for translating these findings into clinically applicable therapies. Comparative studies using different SCI models and varying time-points post-injury would also provide deeper insights into the therapeutic window and durability of the treatment's effects.

Data availability statements

The supplementary data supporting the findings of this study have been uploaded to GitHub and are accessible at the following link: https://github.com/ArmanAbroumand/supplementary-of-SCI/blob/main/Supplementary%20File%20(RPS-39-25%2C%20Final%20Revised%20(Samii).pdf

Acknowledgments

The authors gratefully acknowledge the Vice Chancellery for Research and Technology at Mashhad University of Medical Sciences for providing financial support for this study (Grant No. 995842). We extend our gratitude to Dr. Sara Hosseinian, Dr. Fatemeh Ghaibi, and Professor Hossein Haghir for their invaluable support and for generously providing access to their laboratory facilities for this research.

Conflict of interest statement

The authors declare no conflicts of interest.

Authors' contributions

A. Rabiei Rad and A. Abroumand Gholami conceived and designed the research; E. Amirazodi and F. Mortazavi Moghadam performed the experiments and acquired the data; T. Mokhtari, R. Kazemi Oskuee, and A. Mahdi Molavi analyzed and interpreted the data. A. Abroumand Gholami provided funding and supervised the project. All authors contributed to drafting and revising the manuscript. All authors have read and approved the finalized article. Each author has fulfilled the authorship criteria and affirms that this article represents honest and original work.

REFERENCES

1. Soltani Zangbar H, Ghadiri T, Vafaee MS, Ebrahimi Kalan A, Karimipour M, Fallahi S, *et al*. A potential entanglement between the spinal cord and hippocampus:theta rhythm correlates with neurogenesis deficiency following spinal cord injury in male rats. J Neurosci Res. 2020;98(12):2451-2467. DOI: 10.1002/jnr.24719.
2. Jure I, Lockhart EF, De Nicola AF, Bellini MJ, Labombarda F. IGF1 gene therapy reversed cognitive

deficits and restored hippocampal alterations after chronic spinal cord injury. Mol Neurobiol. 2021;58(12):6186-6202.
DOI: 10.1007/s12035-021-02545-0.
3. Jure I, Pietranera L, De Nicola AF, Labombarda F. Spinal cord injury impairs neurogenesis and induces glial reactivity in the hippocampus. Neurochem Res. 2017;42(8):2178-2190.
DOI: 10.1007/s11064-017-2225-9.
4. Jure I, De Nicola AF, Encinas JM, Labombarda F. Spinal cord injury leads to hippocampal glial alterations and neural stem cell inactivation. Cell Mol Neurobiol. 2022;42(1):197-215.
DOI: 10.1007/s10571-020-00900-8.
5. Chiaravalloti ND, Weber E, Wylie G, Dyson-Hudson T, Wecht JM. Patterns of cognitive deficits in persons with spinal cord injury as compared with both age-matched and older individuals without spinal cord injury. J Spinal Cord Med. 2020;43(1):88-97.
DOI: 10.1080/10790268.2018.1543103.
6. Xie Z, Huang S, Xie S, Zhou W, Li C, Xing Z, *et al*. Potential correlation between depression-like behavior and the mitogen-activated protein kinase pathway in the rat hippocampus following spinal cord injury. World Neurosurg. 2021;154:e29-38.
DOI: 10.1016/j.wneu.2021.06.093.
7. Xue WK, Zhao WJ, Meng XH, Shen HF, Huang PZ. Spinal cord injury induced Neuregulin 1 signaling changes in mouse prefrontal cortex and hippocampus. Brain Res Bull. 2019;144:180-186.
DOI: 10.1016/j.brainresbull.2018.12.002.
8. Sefiani A, Geoffroy CG. The potential role of inflammation in modulating endogenous hippocampal neurogenesis after spinal cord injury. Front Neurosci. 2021;15:682259,1-31.
DOI: 10.3389/fnins.2021.682259.
9. Fumagalli F, Madaschi L, Caffino L, Marfia G, Di Giulio AM, Racagni G, *et al*. Acute spinal cord injury reduces brain derived neurotrohic factor expression in rat hippocampus. Neuroscience. 2009;159(3): 936-939.
DOI: 10.1016/j.neuroscience.2009.01.030.
10. Soltani Zangbar H, Shahabi P, Vafaee MS, Ghadiri T, Kalan AE, Fallahi S, *et al*. Hippocampal neurodegeneration and rhythms mirror each other during acute spinal cord injury in male rats. Brain Res Bull. 2021;172:31-42.
DOI: 10.1016/j.brainresbull.2021.04.004.
11. Karimzadeh Kalkhoran A, Alipour MR, Jafarzadehgharehziaaddin M, Zangbar HS, Shahabi P. Intersection of hippocampus and spinal cord:a focus on the hippocampal alpha-synuclein accumulation, dopaminergic receptors, neurogenesis, and cognitive function following spinal cord injury in male rats. BMC Neurosci. 2022;23(1):44,1-17.
DOI: 10.1186/s12868-022-00729-5.
12. Hsieh FY, Lin HH, Hsu SH. 3D bioprinting of neural stem cell-laden thermoresponsive biodegradable polyurethane hydrogel and potential in central nervous system repair. Biomaterials. 2015;71:48-57.
DOI: 10.1016/j.biomaterials.2015.08.028.
13. Olson HE, Rooney GE, Gross L, Nesbitt JJ, Galvin KE, Knight A, *et al*. Neural stem cell–and schwann cell–loaded biodegradable polymer scaffolds support axonal regeneration in the transected spinal cord. Tissue Eng Part A. 2009;15(7):1797-1805.
DOI: 10.1089/ten.tea.2008.0364.
14. Shin JE, Jung K, Kim M, Hwang K, Lee H, Kim IS, *et al*. Brain and spinal cord injury repair by implantation of human neural progenitor cells seeded onto polymer scaffolds. Exp Mol Med. 2018;50(4):1-18.
DOI: 10.1038/s12276-018-0054-9.
15. Lis-Bartos A, Szarek D, Krok-Borkowicz M, Marycz K, Jarmundowicz W, Laska J. Microstructure and mechanical properties of PU/PLDL sponges intended for grafting injured spinal cord. Polymers (Basel). 2020;12(11):2693,1-17.
DOI: 10.3390/polym12112693.
16. Raguraman M, Zhou X, Mickymaray S, Alothaim AS, Rajan M. Hesperidin guided injured spinal cord neural regeneration with a combination of MWCNT-collagen-hyaluronic acid composite:*in-vitro* analysis. Int J Pharm. 2024;650(4):123609.
DOI: 10.1016/j.ijpharm.2023.123609.
17. Li X, Liu D, Xiao Z, Zhao Y, Han S, Chen B, *et al*. Scaffold-facilitated locomotor improvement post complete spinal cord injury:Motor axon regeneration versus endogenous neuronal relay formation. Biomaterials. 2019;197:20-31.
DOI: 10.1016/j.biomaterials.2019.01.012.
18. Dai Y, Wang W, Zhou X, li L, Tang Y, Shao M, *et al*. Biomimetic electrospun PLLA/PPSB nanofibrous scaffold combined with human neural stem cells for spinal cord injury repair. ACS Appl Nano Mater. 2023;6(7):5980-5993.
DOI: 10.1021/acsanm.3c00374.
19. Yao S, Yang Y, Li C, Yang K, Song X, Li C, *et al*. Axon-like aligned conductive CNT/GelMA hydrogel fibers combined with electrical stimulation for spinal cord injury recovery. Bioact Mater. A2024;35:534-548.
DOI: 10.1016/j.bioactmat.2024.01.021.
20. Shrestha S, Shrestha BK, Kim JI, Won Ko S, Park CH, Kim CS. Electrodeless coating polypyrrole on chitosan grafted polyurethane with functionalized multiwall carbon nanotubes electrospun scaffold for nerve tissue engineering. Carbon N Y. 2018;136: 430-443.
DOI: 10.1016/j.carbon.2018.04.064.
21. Nabipour M, Mellati A, Abasi M, Barough SE, Karimizade A, Banikarimi P, *et al*. Preparation of bilayer tissue-engineered polyurethane/poly-L-lactic acid nerve conduits and their *in vitro* characterization for use in peripheral nerve regeneration. J Biol Eng. 2024;18(1):16,1-17.
DOI: 10.1186/s13036-024-00412-9.
22. Cui T, Yan Y, Zhang R, Liu L, Xu W, Wang X. Rapid prototyping of a double-layer polyurethane–collagen conduit for peripheral nerve regeneration. Tissue Eng Part C Methods. 2009;15(1):1-9.
DOI: 10.1089/ten.tec.2008.0354.

23. Li YM, Patel KD, Han YK, Hong SM, Meng YX, Lee HH, *et al*. Electroconductive and mechano-competent PUCL@CNT nanohybrid scaffolds guiding neuronal specification of neural stem/progenitor cells. Chem Eng J. 2023;466:143125. DOI: 10.1016/j.cej.2023.143125.
24. Wang J, Chu R, Ni N, Nan G. The effect of Matrigel as scaffold material for neural stem cell transplantation for treating spinal cord injury. Sci Rep. 2020;10(1):2576,1-11. DOI: 10.1038/s41598-020-59148-3.
25. Wu J, Zhao Z, Sabirzhanov B, Stoica BA, Kumar A, Luo T, *et al*. Spinal cord injury causes brain inflammation associated with cognitive and affective changes:role of cell cycle pathways. J Neurosci. 2014;34(33):10989-10006. DOI: 10.1523/JNEUROSCI.5110-13.2014.
26. Wang X, Jiao X, Liu Z, Li Y. Crocetin potentiates neurite growth in hippocampal neurons and facilitates functional recovery in rats with spinal cord injury. Neurosci Bull. 2017;33:695-702. DOI: 10.1007/s12264-017-0157-7.
27. Heo SD, Kim J, Choi Y, Ekanayake P, Ahn M, Shin T. Hesperidin improves motor disability in rat spinal cord injury through anti-inflammatory and antioxidant mechanism via Nrf-2/HO-1 pathway. Neurosci Lett. 2020;715:134619,1-8. DOI: 10.1016/j.neulet.2019.134619.
28. Gao C, Li Y, Liu X, Huang J, Zhang Z. 3D bioprinted conductive spinal cord biomimetic scaffolds for promoting neuronal differentiation of neural stem cells and repairing of spinal cord injury. Chem Eng J. 2023 451:138788. DOI: 10.1016/j.cej.2022.138788.
29. Mandour DA, Bendary MA, Alsemeh AE. Histological and imunohistochemical alterations of hippocampus and prefrontal cortex in a rat model of Alzheimer like-disease with a preferential role of the flavonoid "hesperidin." J Mol Histol. 2021;52(5):1043-1065. DOI: 10.1007/s10735-021-09998-6.
30. Matias I, Diniz LP, Buosi A, Neves G, Stipursky J, Gomes FCA. Flavonoid hesperidin induces synapse formation and improves memory performance through the astrocytic TGF-β1. Front Aging Neurosci. 2017 9:184,1-14. DOI: 10.3389/fnagi.2017.00184.
31. Bansal K, Singh V, Singh S, Mishra S. Neuroprotective potential of hesperidin as therapeutic agent in the treatment of brain disorders:preclinical evidence-based review. Curr Mol Med. 2024;24(3):316-326. DOI: 10.2174/1566524023666230320144722.
32. Nones J, e Spohr TCL de S, Gomes FCA. Hesperidin, a flavone glycoside, as mediator of neuronal survival. Neurochem Res. 2011;36(10):1776-1784. DOI: 10.1007/s11064-011-0493-3.
33. Zhang Y, Chen X, Wang X, Xu Y, Li J, Wu Y, *et al*. Hesperetin ameliorates spinal cord injury in rats through suppressing apoptosis, oxidative stress and inflammatory response. Eur J Pharmacol . 2024;971:176541. DOI: 10.1016/j.ejphar.2024.176541
34. Naewla S, Prajit R, Sritawan N, Suwannakot K, Sirichoat A, Aranarochana A, *et al*. Hesperidin ameliorates impairment in hippocampal neural stem cells related to apoptosis induced by methotrexate in adult rats. Biomed Pharmacother. 2023;166:115329. DOI: 10.1016/j.biopha.2023.115329.
35. Najafi Z, Einafshar E, Mirzavi F, Amiri H, Jalili-Nik M, Soukhtanloo M. Protective effect of hesperidin-loaded selenium nanoparticles stabilized by chitosan on glutamate-induced toxicity in PC12 cells. J Nanoparticle Res. 2023;25(9):178. DOI: 10.1007/s11051-023-05828-w.
36. Mokhtari T, Taheri MN, Akhlaghi S, Aryannejad A, Xiang Y, Mahajan V, *et al*. Enhanced epigenetic modulation via mRNA-encapsulated lipid nanoparticles enables targeted anti-inflammatory control. bioRxiv. 2025;639996:1-41. DOI: 10.1101/2025.02.24.639996.
37. Altunayar-Unsalan C, Unsalan O, Mavromoustakos T. Molecular interactions of hesperidin with DMPC/cholesterol bilayers. Chem Biol Interact. 2022;366:110131. DOI: 10.1016/j.cbi.2022.110131.
38. Zhuang H, Zhang X, Wu S, Mao C, Dai Y, Yong P, *et al*. Study transport of hesperidin based on the DPPC lipid model and the BSA transport model. Spectrochim Acta Part A Mol Biomol Spectrosc. 2024;314:124172. DOI: 10.1016/j.saa.2024.124172.
39. Mohammadi M, Alibolandi M, Abnous K, Salmasi Z, Jaafari MR, Ramezani M. Fabrication of hybrid scaffold based on hydroxyapatite-biodegradable nanofibers incorporated with liposomal formulation of BMP-2 peptide for bone tissue engineering. Nanomedicine. 2018;14(7):1987-1997. DOI: 10.1016/j.nano.2018.06.001.
40. Abroumand Gholami A, Gheybi F, Molavi AM, Tahmasebi F, Papi A, Babaloo H. Effect of polycaprolactone/carbon nanotube scaffold implantation along with liposomal ellagic acid in hippocampal synaptogenesis after spinal cord injury. Nanomedicine J. 2023;10(3):197-209. DOI: 10.22038/NMJ.2023.72151.1776.
41. Oyinbo CA. Secondary injury mechanisms in traumatic spinal cord injury:a nugget of this multiply cascade. Acta Neurobiol Exp (Wars). 2011;71(2):281-299. DOI: 10.55782/ane-2011-1848.
42. Paxinos G, Watson CRR, Emson PC. AChE-stained horizontal sections of the rat brain in stereotaxic coordinates. J Neurosci Methods. 1980;3(2):129-149. DOI: 10.1016/0165-0270(80)90021-7.
43. Ma Y, Qiao Y, Gao X. Potential role of hippocampal neurogenesis in spinal cord injury induced post-trauma depression. Neural Regen Res. 2024;19(10):2144-2156. DOI: 10.4103/1673-5374.392855.
44. Li X, Liu S, Zhao Y, Li J, Ding W, Han S, *et al*. Training neural stem cells on functional collagen scaffolds for severe spinal cord injury repair. Adv Funct Mater. 2016;26(32):5835-5847. DOI: 10.1002/adfm.201601521.

45. Haus DL, López-Velázquez L, Gold EM, Cunningham KM, Perez H, Anderson AJ, *et al*. Transplantation of human neural stem cells restores cognition in an immunodeficient rodent model of traumatic brain injury. Exp Neurol. 2016;281:1-16. DOI: 10.1016/j.expneurol.2016.04.008.
46. Veloso AD, Ferraria AM, Botelho do Rego AM, Tavares PB, Valentão P, Pereira DD, *et al*. Hydrophilic carbon nanomaterials:characterisation by physical, chemical, and biological assays. ChemMedChem. 2019;14(6):699-711. DOI: 10.1002/cmdc.201900003.
47. Yu D, Neeley WL, Pritchard CD, Slotkin JR, Woodard EJ, Langer R, *et al*. Blockade of peroxynitrite-induced neural stem cell death in the acutely injured spinal cord by drug-releasing polymer. Stem Cells. 2009;27(5):1212-1222. DOI: 10.1002/stem.26.
48. Park D, Lee HJ, Joo SS, Bae DK, Yang G, Yang YH, *et al*. Human neural stem cells over-expressing choline acetyltransferase restore cognition in rat model of cognitive dysfunction. Exp Neurol. 2012;234(2):521-526. DOI: 10.1016/j.expneurol.2011.12.040.
49. Aranarochana A, Kaewngam S, Anosri T, Sirichoat A, Pannangrong W, Wigmore P, *et al*. Hesperidin reduces memory impairment associated with adult rat hippocampal neurogenesis triggered by valproic acid. Nutrients. 2021;13(12):4364,1-16. DOI: 10.3390/nu13124364.
50. Hassanzadeh A, Yegdaneh A, Rabbani M. Effects of hydroalcoholic, methanolic, and hexane extracts of brown algae Sargassum angustifolium on scopolamine-induced memory impairment and learning deficit in rodents. Res Pharm Sci. 2023;18(3):292-302. DOI: 10.4103/1735-5362.371585.
51. Alipourfard F, Shajiee H, Nazari-Serenjeh F, Hojati V, Alirezaie M. Betaine attenuates oxidative stress and cognitive dysfunction in an amyloid β-induced rat model of Alzheimer's disease. Res Pharm Sci. 2023;18(3):270-278. DOI: 10.4103/1735-5362.371583.
52. Welbat JU, Naewla S, Pannangrong W, Sirichoat A, Aranarochana A, Wigmore P. Neuroprotective effects of hesperidin against methotrexate-induced changes in neurogenesis and oxidative stress in the adult rat. Biochem Pharmacol. 2020;178: 114083,1-9. DOI: 10.1016/j.bcp.2020.114083.
53. Sato K, Sato T, Ohno-Oishi M, Ozawa M, Maekawa S, Shiga Y, *et al*. CHOP deletion and anti-neuroinflammation treatment with hesperidin synergistically attenuate NMDA retinal injury in mice. Exp Eye Res. 2021;213:108826,1-9. DOI: 10.1016/j.exer.2021.108826.
54. Kakebaraei S, Gholami M, Nasta TZ, Arkan E, Bahrehmand F, Fakhri S, Jalili C. Oral administration of crocin-loaded solid lipid nanoparticles inhibits neuroinflammation in a rat model of epileptic seizures by activating SIRT1 expression. Res Pharm Sci. 2024;19(4): 397-414. DOI: 10.4103/RPS.RPS_68_24.